Deconstruction of Resolution Effects in Angle-Resolved Photoemission

G. Levy,[1,2,*] W. Nettke,[1] B. M. Ludbrook,[1] C. N. Veenstra,[1] and A. Damascelli[1,2]

[1] *Department of Physics & Astronomy, University of British Columbia, Vancouver, British Columbia V6T 1Z1, Canada*
[2] *Quantum Matter Institute, University of British Columbia, Vancouver, British Columbia V6T 1Z4, Canada*

(Dated: June 10, 2013)

We study how the energy and momentum resolution of angle-resolved photoemission spectroscopy (ARPES) affects the linewidth, Fermi crossing, velocity, and curvature of the measured band structure. Based on the fact that the resolution smooths out the spectra, and therefore acts as a low-pass filter, we develop an iterative simulation scheme which compensates for resolution effects and allows the fundamental physical parameters to be accurately extracted. By simulating a realistic band structure, we have verified that this method works for an energy resolution up to 100 meV and a momentum resolution equal to twice the energy resolution scaled by the Fermi velocity. Our analysis acquires particular relevance in the hard and soft X-ray regimes, where a degraded resolution limits the accuracy of the extracted physical parameters, and therefore opens a path to study how the electronic excitations are modified when the ARPES probing depth increases beyond the surface.

PACS numbers: 79.60.-i, 73.20.At

I. INTRODUCTION

The electronic excitations at the surface of solids can differ from those in the bulk because the three-dimensional translational symmetry—inherent to the periodic arrangement of atoms that constitutes a solid—is broken.[1–4] This highlights the need for experimental techniques that can probe the evolution of the electronic excitations from surface to bulk, and provide reliable information about the bulk electronic structure. Angle-resolved photoemission spectroscopy (ARPES) can be such a probe, owing to the possibility of progressively increasing the probing depth by varying the photon energy from the UV to the soft and hard X-ray regimes.[5,6] In addition to an increased bulk sensitivity, ARPES at high photon energies also enables the study of the fully-developed three dimensional dispersion in the bulk, extraction of element-specific electronic information by means of resonant photoemission spectroscopy, probing the quantum interference between the decay of photoexcited core-holes and the excitations around the Fermi level, and gaining access to free-electron final states for the photoexcitation process.[6] However, in varying the photon energy from the UV to X-ray regimes, and based on current technical capabilities of ARPES, we face a critical dichotomy for the experimental study of electronic excitations in novel complex materials: on the one hand, working with UV photons achieves the highest energy and momentum resolutions, but also provides the highest sensitivity to the surface electronic structure; on the other hand, the soft and hard X-ray regimes probe deeper into the bulk, avoiding potential surface-related complications,[5,6] but with worse resolution.

In the UV-regime, the energy and angular resolutions $\Delta\omega{\sim}1$ meV and $\Delta\theta{\sim}0.1^\circ$ achieved by ARPES allow the extraction of the electronic self-energy for electrons with binding energy $\omega < 10$ meV with respect to the Fermi energy E_F,[7,8] and also the study of the opening of superconducting gaps as small as $\sim$1 meV and their momentum dependence along the normal state Fermi surface.[9] For example, the use of UV lasers has allowed the measurement of the superconducting gap of $CeRu_2$ with a record-high energy resolution of $\Delta\omega = 0.36$ meV.[10] However, the information obtained in this regime is mainly representative of a material's surface due to the short inelastic mean free path of the photoexcited electrons.[5] Instead, soft and hard X-rays probe deeper into the bulk, but the resolution is degraded by a factor of 10-to-100 as compared to the UV-regime. This resolution degradation affects the observed energy–momentum dispersion relation ϵ_k and electronic lifetime, and limits our ability to observe and analyse the low-energy (*i.e.* $\omega < 0.2$ eV) electronic excitations in solids.

As for the origin of this resolution degradation, we note that in ARPES experiments the total energy resolution $\Delta\omega$ is given by the sum in quadrature of electron-analyzer and photon-beam contributions. In the soft and hard X-ray regime, which requires the use of synchrotron radiation to attain the necessary high photon flux and energy, the ultimate energy resolution is typically limited by the beamline monochromator contribution, $\Delta h\nu$, defined by its resolving power $R_m = h\nu/\Delta h\nu$. State-of-the-art soft X-ray beamlines can achieve a resolving power as good as $R_m \simeq 33,000$ for photon energies $h\nu \simeq 1$ keV, corresponding to an ultimate energy resolution of $\Delta h\nu \simeq 30$ meV.[11] As for the total momentum resolution Δk, this is mainly determined by the angular resolution of the detector and the kinetic energy of the photoelectrons.[5,12] For a $\Delta\theta \simeq 0.1^\circ$ angular resolution, the momentum resolution varies from $\Delta k \simeq 4\times10^{-4}$ Å^{-1} in the UV-regime ($h\nu \simeq 16$ eV) to 3×10^{-3} Å^{-1} in the X-ray regime ($h\nu \simeq 900$ eV).

Attempts to mitigate the effects of poor energy and momentum resolution on the determination of the underlying physical parameters of a system can be classified into three groups: i) comparison between experimental results and theoretical calculations where the experimental resolutions are included;[13] ii) deconvolution

methods, such as Lucy-Richardson or Wiener filters,[14] to reduce the effects of the resolution broadening before any further analysis is performed;[15,16] iii) the combination of a one-dimensional fitting routine with the convolution with an instrumental resolution function.[17,18] Methods in the first group involve a theoretical description of the excitations and are therefore model dependent, while those in the second require a high signal-to-noise ratio since otherwise they would be prevented altogether by the noise magnification during the deconvolution process. The third approach is based on a phenomenological description of the ARPES data; it does not demand the development of a specific model or high signal–to–noise ratio, and will be the one followed here.

In this paper, we present a systematic study of how momentum and energy resolutions affect the observed dispersion and lifetime of the electronic excitations. By performing an analysis of momentum distribution curves (MDCs), obtained as constant energy cuts of the ARPES intensity data, we verify that the momentum resolution is responsible only for an energy-independent contribution to the MDC linewidth, provided it is smaller than the energy resolution scaled by the quasiparticle velocity (we also note that the MDC analysis is only valid for weakly momentum-dependent self-energies). This observation allows us to concentrate on the effects of the energy resolution alone: although the latter hampers a straightforward extraction of the physical quantities when it is larger than 25 meV, we show that those can be recovered using an iterative algorithm, which belongs to the phenomenological third approach mentioned above. As will be discussed later, this new method – called *iterative deconstruction algorithm* – is based on the observation that the main effect of the energy resolution is to act as a low-pass filter on the ARPES signal.

II. SPECTRAL FUNCTION

We start by describing our phenomenological model. The intensity $I(k,\omega)$ of the ARPES signal as a function of electron momentum k and energy ω is written as:[5,17,19]

$$I(k,\omega) = |M_{if}|^2 \left[A(k,\omega) f(\omega,T) + B\right] \otimes R(\Delta k, \Delta\omega), \quad (1)$$

where M_{if} represents the matrix element which accounts for the selection rules for the optical transition between initial and final states, $A(k,\omega)$ is the single-particle spectral function describing the electronic excitations in the solid, $f(\omega,T)$ is the Fermi-Dirac distribution describing the statistical electronic population at temperature T for states with energy ω with respect to the chemical potential, and B is a background. These quantities are convolved with the instrumental resolution function $R(\Delta k, \Delta\omega)$, where Δk and $\Delta\omega$ are the total energy and momentum experimental resolutions. In this study we will neglect quantum interference effects[20] due to the matrix elements $|M_{if}|^2$, which depend on photon polarization and energy, by assuming a constant value; this is equivalent to considering a system where only a single initial-to-final-state transition is allowed. Similarly, we also assume a step-like background B for simplicity.

The spectral function $A(k,\omega)$, describing the single-particle excitation spectrum, can be written as:

$$A(k,\omega) = \frac{1}{\pi} \frac{-\Sigma''(k,\omega)}{\left[\omega - \epsilon_k^b - \Sigma'(k,\omega)\right]^2 + \left[\Sigma''(k,\omega)\right]^2}, \quad (2)$$

where the self-energy $\Sigma(k,\omega) = \Sigma'(k,\omega) + i\Sigma''(k,\omega)$ captures the many-body correlation effects on the electronic excitations, and ϵ_k^b represents the bare-band dispersion. The effects of the self-energy are two-fold: the real part of the self-energy renormalizes the bare-band dispersion ϵ_k^b into the quasiparticle dispersion $\epsilon_k^q = \epsilon_k^b - \Sigma'(k,\omega)$, and the imaginary part $\Sigma"(k,\omega)$ describes the reduction in the lifetime of the single-particle excitations and the corresponding increase of the peak width in energy.

For a weakly momentum-dependent self-energy, the spectral function may be further simplified by replacing $\Sigma(k,\omega)$ with $\Sigma(\omega)$, thus obtaining:

$$A(k,\omega) = \frac{1}{\pi} \frac{\Gamma(\omega)}{\left[\omega - \epsilon_k^q\right]^2 + \left[\Gamma(\omega)\right]^2}. \quad (3)$$

In this case the electron self-energy may be extracted more straightforwardly from the ARPES spectra through Lorentzian fits of the MDCs,[5,21] even without any *a priori* knowledge of the bare-band ϵ_k^b.[22,23] However, the apparent quasiparticle dispersion ϵ_k^q and peak widths $\Gamma(\omega) = -\Sigma''(\omega)/v_k^b$, where $v_k^b = \partial\epsilon_k^b/\partial k$ is the bare-band velocity, will be affected by both momentum and energy experimental resolutions.

We establish here an analogy between the instrumental resolution $R(\Delta k, \Delta\omega)$ and a low-pass filter by considering the influence of resolution in the detection process. When an electron with energy ω and momentum k enters the detector, the instrumental resolution is determined by the probability of detecting it with energy ω' and momentum k'. This probability distribution, represented by $R(\Delta k, \Delta\omega)$ in Eq. 1, decays as $|\omega - \omega'|$ and $|k - k'|$ increase. As a result, the ARPES signal is proportional to the photoemitted electron distribution convolved with the instrumental resolution function $R(\Delta k, \Delta\omega)$. The effect of the instrumental resolution can be modelled as a *low-pass filter* because the resolution effectively smooths out the spectra, suppressing variations of the signal that have a frequency in energy/momentum higher than the resolution itself. Furthermore, the functional form of the experimental resolution $R(\Delta k, \Delta\omega)$ can be approximated by a Gaussian profile,[24,25] and within this approximation the instrumental resolution acting upon the signal is equivalent to a Gaussian filter.

One can show that, when the broadening due to the energy resolution scaled by the quasiparticle velocity is larger than the corresponding broadening due to the momentum resolution, the net effect of the momentum resolution in the MDC analysis is to increase the effective linewidth by an energy-independent value. In particular,

for momentum-independent self-energies the MDC lineshape can be described by a Lorentzian profile,[26] which is modified into a Voigt profile by the convolution with a Gaussian resolution function in momentum.[27] Both curves are difficult to distinguish experimentally for low-to-medium signal-to-noise ratios since the largest difference is in the tails of the profiles, away from the peak position. For this reason, in the rest of the manuscript we restrict the analysis to the case $\Delta k = 0$; note, however, that we have verified that a finite Δk does not alter the results of our analysis when $\Delta k \leq 2\Delta\omega/v_{\rm F}^q$, where $v_{\rm F}^q$ is the quasiparticle Fermi velocity. We also note that this upper limit on the momentum resolution does not imply an experimental limitation on the maximum value of $v_{\rm F}^q$ that can be measured by this technique because, for a given momentum resolution, higher values of $v_{\rm F}^q$ can be accessed by decreasing experimentally the energy resolution. Also, this condition does not imply that different results should be obtained between UV and X-ray regimes because energy and momentum resolutions scale approximately at the same rate with photon energy and, in turn, the resolution ratio $\Delta\omega/\Delta k$ remains comparable.

Under these conditions – and contrary to the momentum resolution – the energy resolution modifies the energy dependence of the parameters obtained from the MDC analysis since it mixes spectral weight from states at different energies. We find that the effects of the energy resolution $\Delta\omega$, as depicted in Fig. 1, are: i) a distortion of the functional form of the resulting dispersion ϵ_k^* with respect to the intrinsic ϵ_k^q in an energy region $\Delta\omega$ around $E_{\rm F}$, as was reported previously;[17] ii) a shift of the peak positions close to $E_{\rm F}$, which results in a different Fermi crossing $k_{\rm F}^*$;[28,29] iii) a modification of the Fermi velocity from $v_{\rm F}^q$ to $v_{\rm F}^*$; iv) an increase of MDC linewidth, $\Gamma(\omega)$, inversely proportional to the slope of the band dispersion; v) a reduction of the average-rate-of-change of the linewidth with energy.

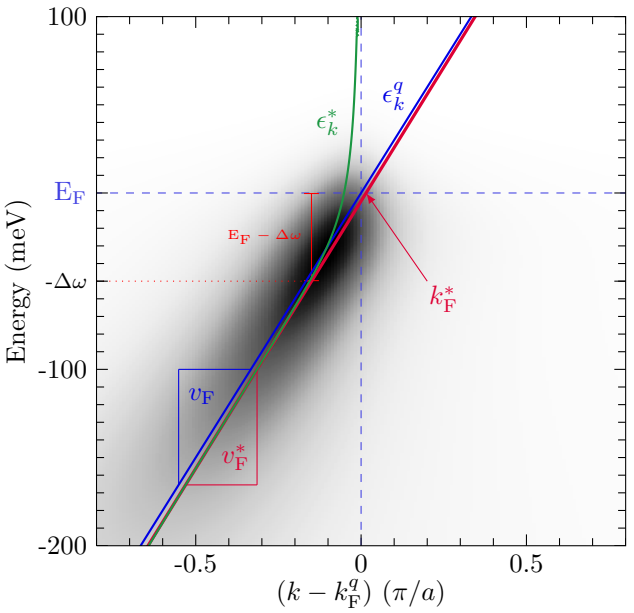

FIG. 1. (Color online) Effect of energy resolution on a linear dispersion with Fermi-liquid linewidth. The gray scale ARPES intensity is obtained from Eqs. 1 and 3 for $T = 10\,\mathrm{K}$, $\Delta\omega = 50\,\mathrm{meV}$, and $\Delta k = 0$, using the quasiparticle dispersion $\epsilon_k^q = v_{\rm F}^q(k - k_{\rm F}^q)$ (blue line) and linewidth $\Gamma(\omega) = \Gamma_0 + \Gamma_2\,\omega^2$, with $v_{\rm F}^q = 1\,\mathrm{eV}\,a/\pi$, $\Gamma_0 = 0.1\,\pi/a$, and $\Gamma_2 = 10\,\mathrm{eV}^{-2}\,\pi/a$ (all quantities including k expressed in units of π/a). The extracted dispersion ϵ_k^* (green line) is obtained from the Lorentzian fit of the MDCs; Fermi momentum $k_{\rm F}^*$ and velocity $v_{\rm F}^*$ from a linear fit of ϵ_k^* up to $E_{\rm F} - \Delta\omega$ (red line).

III. RESOLUTION EFFECTS

A. Linear quasiparticle dispersion

To illustrate the resolution effects alluded to above, we simulate the spectral function $A(k,\omega)$ using a linear quasiparticle band $\epsilon_k^q = v_{\rm F}^q(k - k_{\rm F}^q)$ with a corresponding Fermi liquid energy-dependent width $\Gamma(\omega) = \Gamma_0 + \Gamma_2\,\omega^2$, where Γ_0 and Γ_2 account for impurity and electron-electron scattering, respectively. As described in Eq. 1, the spectral function is multiplied by the Fermi-Dirac distribution and then convolved with a Gaussian energy resolution function with unit-area and full-width half-maximum (FWHM) equal to $\Delta\omega$. An example of such simulation is shown as a gray scale plot in Fig. 1, with the linear dispersion ϵ_k^q in blue. Here we used an energy resolution $\Delta\omega = 50\,\mathrm{meV}$, a momentum resolution $\Delta k = 0$, a Fermi velocity $v_{\rm F}^q = 1\,\mathrm{eV}\,a/\pi$, and linewidth parameters $\Gamma_0 = 0.1\,\pi/a$ and $\Gamma_2 = 10\,\mathrm{eV}^{-2}\,\pi/a$. We note that throughout the paper all dispersion-related quantities – including the electron momentum k – are expressed in units of π/a, where a is the lattice parameter; also, the temperature was set to 10 K for all simulations.

Fitting the corresponding MDCs with a Lorentzian profile we obtain the dispersion ϵ_k^* (green line in Fig. 1), which is identical to the quasiparticle dispersion ϵ_k^q only when $\Delta\omega = 0$. When the energy broadening part of the resolution function is larger than the width of the Fermi-Dirac distribution ($\Delta\omega > 4k_BT$),[17] ϵ_k^* deviates from the linearly dispersive band ϵ_k^q for energies closer to $E_{\rm F}$ than $\Delta\omega$, showing an upturn above this energy. The interplay of energy resolution and spectral cut-off due to the Fermi-Dirac distribution is at the origin of these effects, as well as of the spectral weight induced above $E_{\rm F}$ and extending up to $E_{\rm F} + \Delta\omega$. Practically, the deviation of ϵ_k^* from ϵ_k^q in the range $|E_{\rm F} - \Delta\omega|$ defines the maximum binding energy at which the band dispersion can be accurately traced; this also provides a method to estimate the energy resolution directly from the data: $\Delta\omega$ corresponds to the energy relative to $E_{\rm F}$ where the upturn in ϵ_k^* has its onset.

At binding energies below the $\Delta\omega$ range around $E_{\rm F}$, the extracted band dispersion ϵ_k^* is linear but is shifted compared to ϵ_k^q, as shown by the comparison of green and blue lines in Fig. 1. This shift is caused by the inter-

play of the energy resolution with the quadratic energy-dependence of the MDC linewidth, which induces an asymmetry in the MDC profiles; when this asymmetric lineshape is fitted with a Lorentzian function, the result is a shift in peak position. This would not occur if there were only an energy-independent term in the momentum width $\Gamma = \Gamma_0$, or if the energy resolution broadening were reduced to $\Delta\omega = 0$ (as shown below, a similar shift of the peak positions also occurs for non-linear dispersions). As reported previously,[28,29] in Fig. 1 we can also see that as a consequence of this shift, the extrapolated Fermi momentum $k_{\rm F}^*$ moves with respect to $k_{\rm F}^q$, affecting the determination of the Fermi surface in an MDC analysis [this will be discussed in greater detail in relation to Fig. 2(b)].

Next we study the variation, due to the energy resolution, of the extracted Fermi velocity $v_{\rm F}^*$, as obtained from a linear fit of the dispersion ϵ_k^* up to $E_{\rm F} - \Delta\omega$. The deviation of the Fermi velocity $v_{\rm F}^*$ from the intrinsic $v_{\rm F}^q$ depends on the interplay of temperature T, linewidth Γ, and energy resolution $\Delta\omega$. Note that for zero energy resolution, $v_{\rm F}^* = v_{\rm F}^q$ independent of the other parameters, which demonstrates that its deviation is due to a finite $\Delta\omega$. The relative velocity $v_{\rm F}^r = v_{\rm F}^*/v_{\rm F}^q$ increases quadratically with the energy resolution; and for a given energy resolution, $v_{\rm F}^r$ increases quadratically with temperature, semi-logarithmically with the input Fermi velocity $v_{\rm F}^q$, and semi-logarithmically with the energy-independent momentum width Γ_0. In absolute terms, the deviations of $v_{\rm F}^*$ due to temperature (up to 100 K) and energy-independent momentum width term Γ_0 (up to $2\Delta\omega/v_{\rm F}^q$) are at most 6%. As expected, the largest contribution is due to $\Delta\omega$. The increase of the extracted Fermi velocity $v_{\rm F}^*$ with energy resolution $\Delta\omega$ can be understood by the smoothing effect mentioned in the low-pass filter analogy: $\Delta\omega$ introduces an effective cut-off for the maximum rate-of-change observable in the energy distribution curves (EDCs); this EDC broadening, together with the quadratic energy dependence of the linewidth, translates into an increase of $v_{\rm F}^*$ inferred from the MDC analysis. As a limiting case, we expect that $v_{\rm F}^* \to \infty$ when $\Delta\omega \to \infty$.

B. Quadratic quasiparticle dispersion

Following the same approach, we also expect that the effect of energy resolution on a parabolic band dispersion is to reduce its curvature. This point is exemplified in Fig. 2, where we consider the change of the extracted spectroscopic quantities due to energy resolution for the quasiparticle dispersion $\epsilon_k^q = \frac{\hbar^2}{2m}(k - k_{\rm F}^q)^2 + v_{\rm F}^q(k - k_{\rm F}^q)$ and a Fermi-liquid linewidth $\Gamma = \Gamma_0 + \Gamma_2\omega^2$. From the ARPES intensity $I(k,\omega)$ in Fig. 2(a), calculated for the parameter values indicated in the caption, we extract the quasiparticle dispersion ϵ_k^* (green line) affected by the energy resolution; this can be tracked up to $E_{\rm F} - \Delta\omega$ before it deviates from the intrinsic ϵ_k^q dispersion. By fitting

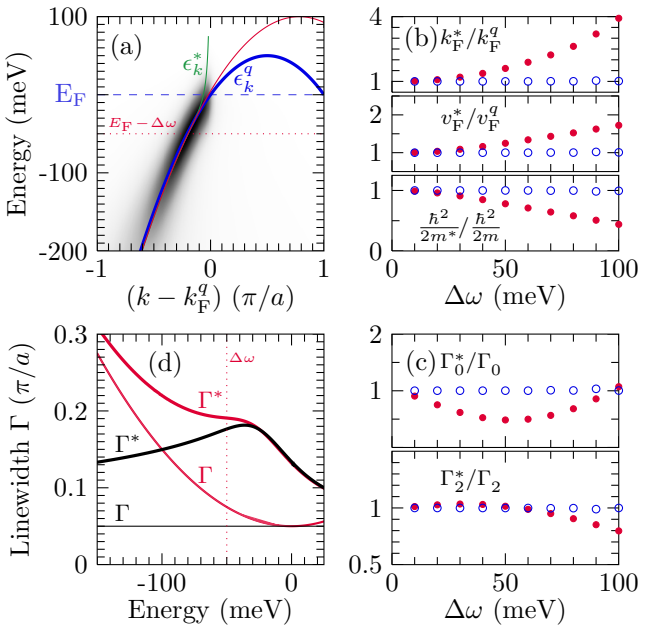

FIG. 2. (Color online) Effect of energy resolution on a parabolic dispersion with Fermi-liquid linewidth. (a) The gray scale ARPES intensity is obtained from Eqs. 1 and 3, for $T = 10$ K, $\Delta\omega = 50$ meV, and $\Delta k = 0$, using the quasiparticle dispersion $\epsilon_k^q = \frac{\hbar^2}{2m}(k - k_{\rm F}^q)^2 + v_{\rm F}^q(k - k_{\rm F}^q)$ (blue line) and linewidth $\Gamma = \Gamma_0 + \Gamma_2\omega^2$, with $v_{\rm F}^q = 0.2\,{\rm eV}\,a/\pi$, $\Gamma_0 = 0.1\,\pi/a$, $\hbar^2/2m = -0.2\,{\rm eV}\,(a/\pi)^2$, $\Gamma_0 = 0.1\,\pi/a$, and $\Gamma_2 = 10\,{\rm eV}^{-2}\,\pi/a$ (all quantities including k expressed in units of π/a). The green line is the dispersion ϵ_k^* extracted from the MDC analysis; the red one is the result of a quadratic fit of ϵ_k^* at binding energies deeper than $E_{\rm F} - \Delta\omega$. (b) Energy-resolution dependence of the parameters (solid red symbols) $k_{\rm F}^*$, $v_{\rm F}^*$, and $\hbar^2/2m^*$, and (c) Γ_0^* and Γ_2^*, as determined by fitting the band dispersion ϵ_k^* [green line in (a)] obtained from an MDC analysis of the ARPES intensity in (a); open symbols are the results of the iterative deconstruction algorithm discussed in Sec. IV. (d) The linewidth Γ^* deviates from the input linewidth Γ (red lines), even in the case of a purely constant input $\Gamma = \Gamma_0$ (black lines).

ϵ_k^* with a parabolic dispersion outside of the $\Delta\omega$ energy range, we obtain the red line in Fig. 2(a), from which we can extract estimates for the Fermi momentum $k_{\rm F}^*$, Fermi velocity $v_{\rm F}^*$, and quasiparticle curvature $\hbar^2/2m^*$. As shown by the red filled symbols in Fig. 2(b), these extracted parameters vary quadratically with energy resolution relative to the input values $k_{\rm F}^q$, $v_{\rm F}^q$, and $\hbar^2/2m^*$, which are instead recovered for $\Delta\omega = 0$. The variation of the extracted Fermi velocity $v_{\rm F}^*$ and curvature $\hbar^2/2m^*$ with $\Delta\omega$ follows the guideline previously stated that the energy resolution tends to smooth out the ARPES spectra: it reduces the overall curvature and increases the Fermi velocity [see Fig. 2(b)]. As a result, the extracted Fermi momentum $k_{\rm F}^*$ (decreases) increases with $\Delta\omega$ for (electron-) hole-like Fermi surfaces.

As for the energy-resolution dependence of the extracted linewidth $\Gamma^* = \Gamma_0^* + \Gamma_2^*\omega^2$, in Fig. 2(c) we observe

that the relative variation of the energy-independent Γ_0^* and quadratic Γ_2^* are non-monotonic with the energy resolution $\Delta\omega$ (see red filled symbols, and again $\Delta\omega = 0$ for the input values). In addition, the energy-dependence of Γ^* is modified by a term inversely proportional to the slope of the quasiparticle dispersion ϵ_k^q. To illustrate this, we consider first an energy-independent momentum width $\Gamma \equiv \Gamma_0$ as a simpler case. The MDC Lorentzian profile of width Γ_0 is modified into a Voigt lineshape by the convolution with a Gaussian function of width $\sigma_g(E) \propto \Delta\omega/(\partial\epsilon_k/\partial k)|_\omega$. Remarkably [see black lines in Fig. 2(d)], the extracted Γ^* exhibits an energy dependence although the input linewidth $\Gamma = \Gamma_0$ is constant in energy. In case of the quadratic linewidth $\Gamma = \Gamma_0 + \Gamma_2\omega^2$ [see red lines in Fig. 2(d)], the extracted Γ^* still presents a parabolic dependence on energy for $\omega < E_F - \Delta\omega$, but deviates considerably from the input linewidth Γ.

IV. ITERATIVE DECONSTRUCTION ALGORITHM

So far, we have analysed the variation with energy resolution of the quantities k_F^*, v_F^*, $\hbar^2/2m^*$, Γ_0^*, and Γ_2^*, which parametrize the electronic dispersion ϵ_k^* and lifetime Γ^* obtained from an MDC analysis of the ARPES intensity. We have shown that these variations can be understood as a cut-off on the maximum rate-of-change of the ARPES intensity imposed by the experimental resolutions, in analogy with a low-pass filter effect. This becomes more pronounced the stronger the energy dependence of the quasiparticle dispersion. For example, as shown in Fig. 3(a) and (b), the resolution-induced deviations of the extracted Fermi velocity v_F^* and especially curvature $|\hbar^2/2m^*|$ increase with the input parameters; this observation can be generalized to each dispersion parameter p, to show that the absolute difference between extracted and intrinsic values, $|p - p^*|$, increases with p.

Based on this observation we devise an iterative method to retrieve the intrinsic parameters p, starting from the p^* extracted – and affected by the experimental resolution – through the MDC analysis of the *measured* ARPES intensity $I(k, \omega)$. The iterations are initialized defining the first set of parameters to be identical to the *measured* ones, $p_1 \equiv p^*$. Next, using this set of p_1 and the known energy resolution, a *simulated* ARPES intensity map is generated; new values for the parameters p_1^* can then be extracted, now through an MDC analysis of the *simulated* intensity. Note that these newly determined p_1^* will be further away from the intrinsic parameters p than the input values $p_1 \equiv p^*$, due to the energy resolution broadening having effectively been accounted for twice. By taking the difference $\Delta_1 = p_1 - p_1^*$, and subtracting it from the *measured* p^*, we define the starting parameters for the next iteration: $p_2 = p^* - \Delta_1$. As a result of the second iteration, we obtain the new difference $\Delta_2 = p_2 - p_2^*$ and then the input values for the third iteration: $p_3 = p^* - \Delta_2$. These iterations are repeated

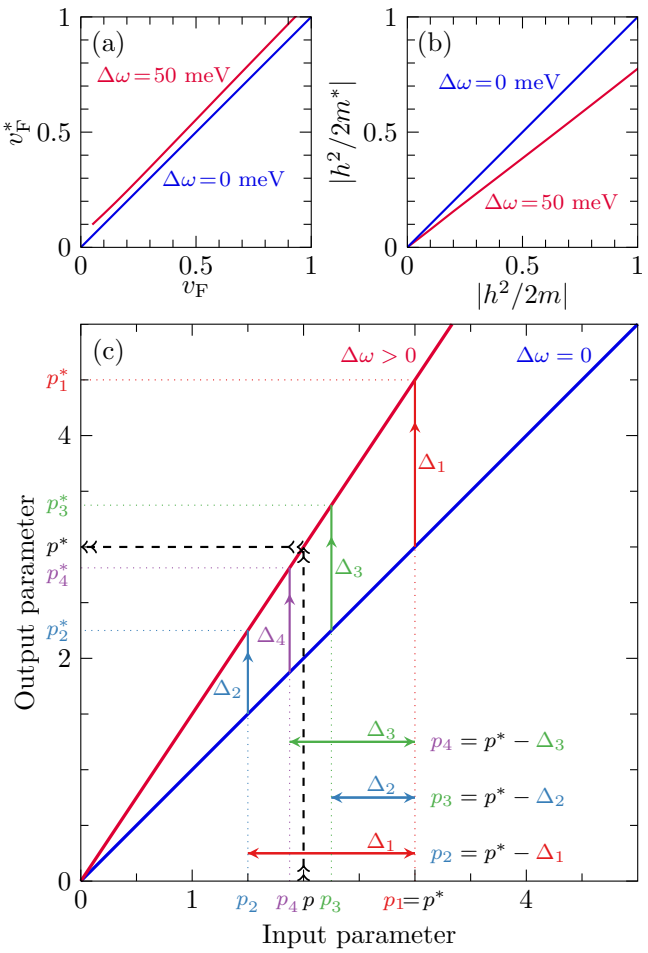

FIG. 3. (Color online) Iterative deconstruction algorithm to retrieve the intrinsic parameters p from the p^* as *measured* – and modified by the energy resolution. At a constant energy resolution $\Delta\omega = 50$ meV, the energy-resolution-induced deviations of (a) Fermi velocity v_F^* and (b) band curvature $|\hbar^2/2m^*|$ from the corresponding input values increase with the magnitude of the latter; note that here all other parameters are the same as in Fig. 2(a). The iterative deconstruction algorithm is illustrated in (c), and shows that starting from the *measured* parameters $p_1 \equiv p^*$, the iterative input (p_i) and extracted (p_i^*) parameters progressively converge towards the true (p) and measured values (p^*); note that here $\Delta_i = p_i - p_i^*$. The iteration is stopped when the difference between p_i^* and p^* is smaller than an appropriate tolerance factor.

until the difference between the output values p_i^* and the *measured* p^* is below a chosen tolerance factor. At this point, the input parameters p_i of the last iteration, can be considered representative of the true values p. The key iterative steps, with $i = 1, 2, ...$, are thus

$$\begin{aligned} p_1 &= p^*, \\ \Delta_i &= p_i - p_i^*, \\ p_{i+1} &= p^* - \Delta_i, \end{aligned} \tag{4}$$

Note that the difference Δ_i is always combined with the *measured* parameters p^* for all iterations; this is nec-

essary because the information of the true values p is encoded in the measured values p^* together with the energy resolution $\Delta\omega$. This iterative deconstruction algorithm is illustrated in Fig. 3(c), and shows how the input (p_i) and extracted (p_i^*) parameters progressively converge towards the true (p) and measured (p^*) values. By applying the iterative deconstruction algorithm to the example discussed before of a parabolic band dispersion with a Fermi-liquid linewidth, we find that the systematic error induced by the energy resolution is reduced to $< 3\%$, as shown by the open circles in Fig. 2(b) and (c). Finally, one should note that this method only relies on the monotonous increase of $|p_i - p_i^*|$ with p_i, and not on its specific functional form.

V. CONCLUSIONS

We systematically studied the effect of energy resolution on the measured MDC linewidth and quasiparticle dispersion parameters, such as Fermi velocity, Fermi momentum, and band curvature, as extracted from ARPES data. In particular, we considered the case of linear and parabolic dispersions, with a quadratic Fermi-liquid-like scattering rate. Starting from the observation that the energy resolution acts as a low-pass filter, we developed an iterative deconstruction algorithm to extract the underlying physical parameters, compensating for the progressive loss of energy resolution upon increasing of photon energy from the UV to hard X-ray regime. This method provides an avenue for studying the electronic excitations with enhanced bulk sensitivity and to follow their bulk-to-surface evolution, with the highest degree of fidelity despite the reduced instrumental energy resolution, i.e. with an accuracy better than the energy resolution itself. Note however that this method relies on the trend of the MDC lineshape at energies at least twice as large as the energy resolution $\Delta\omega$; therefore, it cannot provide information on features pertaining to a scale smaller than $\Delta\omega$. This method could be generalized to other parametrizations and techniques where energy resolution produces similar effects, such as angle-resolved bremsstrahlung isochromat spectroscopy; however, its applicability should be verified case by case.

ACKNOWLEDGMENTS

We thank G.A. Sawatzky and I.S. Elfimov for their critical questions which motivated this study. This work was supported by the Killam, Alfred P. Sloan, and NSERC's Steacie Memorial Fellowships (A.D.), the Canada Research Chairs Program (A.D.), NSERC, CFI, and CIFAR Quantum Materials.

* giorgio.levy@phas.ubc.ca

[1] R. Matzdorf, Z. Fang, Ismail, J. Zhang, T. Kimura, Y. Tokura, K. Terakura, and E. W. Plummer, Science **289**, 746 (2000).
[2] P. Echenique, R. Berndt, E. Chulkov, T. Fauster, A. Goldmann, and U. Hfer, Surf. Sci. Rep. **52**, 219 (2004).
[3] D. Fournier, G. Levy, Y. Pennec, J. L. McChesney, A. Bostwick, E. Rotenberg, R. Liang, W. N. Hardy, D. A. Bonn, I. S. Elfimov, and A. Damascelli, Nat Phys **6**, 905 (2010).
[4] C. N. Veenstra, Z.-H. Zhu, B. Ludbrook, M. Capsoni, G. Levy, A. Nicolaou, J. A. Rosen, R. Comin, S. Kittaka, Y. Maeno, I. S. Elfimov, and A. Damascelli, Phys. Rev. Lett. **110**, 097004 (2013).
[5] A. Damascelli, Phys. Scripta **2004**, 61 (2004).
[6] C. S. Fadley, Synchroton Radiat. News **25**, 26 (2012).
[7] N. C. Plumb, T. J. Reber, J. D. Koralek, Z. Sun, J. F. Douglas, Y. Aiura, K. Oka, H. Eisaki, and D. S. Dessau, Phys. Rev. Lett. **105**, 046402 (2010).
[8] A. Tamai, W. Meevasana, P. D. C. King, C. Nicholson, A. de la Torre, E. Rozbicki, and F. Baumberger, (2013), arxiv:1301.5991.
[9] K. Umezawa, Y. Li, H. Miao, K. Nakayama, Z.-H. Liu, P. Richard, T. Sato, J. B. He, D.-M. Wang, G. F. Chen, H. Ding, T. Takahashi, and S.-C. Wang, Phys. Rev. Lett. **108**, 037002 (2012).
[10] T. Kiss, F. Kanetaka, T. Yokoya, T. Shimojima, K. Kanai, S. Shin, Y. Onuki, T. Togashi, C. Zhang, C. T. Chen, and S. Watanabe, Phys. Rev. Lett. **94**, 057001 (2005).
[11] V. N. Strocov, T. Schmitt, U. Flechsig, T. Schmidt, A. Imhof, Q. Chen, J. Raabe, R. Betemps, D. Zimoch, J. Krempasky, X. Wang, M. Grioni, A. Piazzalunga, and L. Patthey, J. Synchrotron Rad. **17**, 631 (2010).
[12] In ARPES, there are two contributions to the momentum resolution: the angular resolution of the detector and the energy resolution of the monochromator. The relative momentum resolution for momentum parallel to the surface can be expressed as:

$$\frac{\Delta k_{\parallel}}{k_{\parallel}} = \sqrt{[\Delta\theta \cot(\theta)]^2 + R^{-2}},$$

where θ is the polar emission angle defined by the geometry of the experimental setup and R is the monochromator resolving power. The first term, the angular contribution, dominates due to the high resolving power normally achieved, $R_m > 100$.
[13] X. Y. Cui, K. Shimada, Y. Sakisaka, H. Kato, M. Hoesch, T. Oguchi, Y. Aiura, H. Namatame, and M. Taniguchi, Phys. Rev. B **82**, 195132 (2010).
[14] H.-B. Yang, J. Rameau, P. Johnson, T. Valla, A. Tsvelik, and G. Gu, Nature **456**, 77 (2008).
[15] L. Lucy, Astron. J. **79**, 745 (1974).
[16] J. Rameau, H.-B. Yang, and P. Johnson, J. Electron. Spectrosc. Relat. Phenom. **181**, 35 (2010).
[17] N. J. C. Ingle, K. M. Shen, F. Baumberger, W. Meevasana, D. H. Lu, Z.-X. Shen, A. Damascelli, S. Nakatsuji, Z. Q. Mao, Y. Maeno, T. Kimura, and Y. Tokura, Phys. Rev. B **72**, 205114 (2005).

[18] D. V. Evtushinsky, D. S. Inosov, V. B. Zabolotnyy, A. Koitzsch, M. Knupfer, B. Büchner, M. S. Viazovska, G. L. Sun, V. Hinkov, A. V. Boris, C. T. Lin, B. Keimer, A. Varykhalov, A. A. Kordyuk, and S. V. Borisenko, Phys. Rev. B **79**, 054517 (2009).
[19] A. A. Kordyuk, S. V. Borisenko, M. Knupfer, and J. Fink, Phys. Rev. B **67**, 064504 (2003).
[20] Z. H. Zhu, C. N. Veenstra, G. Levy, A. Ubaldini, P. Syers, N. P. Butch, J. Paglione, M. W. Haverkort, I. S. Elfimov, and A. Damascelli, Phys. Rev. Lett. **110**, 216401 (2013), arxiv:1212.4845.
[21] T. Valla, A. V. Fedorov, P. D. Johnson, B. O. Wells, S. L. Hulbert, Q. Li, G. D. Gu, and N. Koshizuka, Science **285**, 2110 (1999).
[22] C. N. Veenstra, G. L. Goodvin, M. Berciu, and A. Damascelli, Phys. Rev. B **82**, 012504 (2010).
[23] C. N. Veenstra, G. L. Goodvin, M. Berciu, and A. Damascelli, Phys. Rev. B **84**, 085126 (2011).
[24] R. E. Imhof, A. Adams, and G. C. King, J. Phys. E: Sci. Instrum. **9**, 138 (1976).
[25] P. Storer, R. S. Caprari, S. A. C. Clark, M. Vos, and E. Weigold, Rev. Sci. Instrum. **65**, 2214 (1994).
[26] M. Randeria, A. Paramekanti, and N. Trivedi, Phys. Rev. B **69**, 144509 (2004).
[27] H. C. van de Hulst and J. J. M. Reesinck, Astrophys. J. **106**, 121 (1947).
[28] L. Kipp, K. Roßnagel, C. Solterbeck, T. Strasser, W. Schattke, and M. Skibowski, Phys. Rev. Lett. **83**, 5551 (1999).
[29] S. V. Borisenko, A. A. Kordyuk, S. Legner, C. Dürr, M. Knupfer, M. S. Golden, J. Fink, K. Nenkov, D. Eckert, G. Yang, S. Abell, H. Berger, L. Forró, B. Liang, A. Maljuk, C. T. Lin, and B. Keimer, Phys. Rev. B **64**, 094513 (2001).